

Arrested phase separation in reproducing bacteria: a generic route to pattern formation?

M. E. Cates,¹ D. Marenduzzo,¹ I. Pagonabarraga,² and J. Tailleur¹

¹*SUPA, School of Physics and Astronomy, University of Edinburgh, Mayfield Road, Edinburgh EH9 3JZ, UK*

²*Departament de Física Fonamental, Universitat de Barcelona - Carrer Martí Franqués 1, 08028-Barcelona, Spain*

(Dated: November 24, 2021)

We present a generic mechanism by which reproducing microorganisms, with a diffusivity that depends on the local population density, can form stable patterns. It is known that a decrease of swimming speed with density can promote separation into bulk phases of two coexisting densities; this is opposed by the logistic law for birth and death which allows only a single uniform density to be stable. The result of this contest is an arrested nonequilibrium phase separation in which dense droplets or rings become separated by less dense regions, with a characteristic steady-state length scale. Cell division mainly occurs in the dilute regions and cell death in the dense ones, with a continuous flux between these sustained by the diffusivity gradient. We formulate a mathematical model of this in a case involving run-and-tumble bacteria, and make connections with a wider class of mechanisms for density-dependent motility. No chemotaxis is assumed in the model, yet it predicts the formation of patterns strikingly similar to those believed to result from chemotactic behavior.

Microbial and cellular colonies are among the simplest examples of self-assembly in living organisms. In nature, bacteria are often found in concentrated biofilms, mats or other colony types, which can grow into spectacular patterns visible under the microscope [1, 2]. Also in the laboratory, bacteria such as *E. coli* and *S. typhimurium* form regular geometric patterns when they reproduce and grow on a Petri dish containing a gel such as agar. These patterns range from simple concentric rings to elaborate ordered or amorphous arrangements of dots [3–6]. Their formation results from collective behaviour driven by interactions between the bacteria, such as chemotactic aggregation [6], competition for food [8] or changes in phenotypes according to density [11]. The question as to whether general mechanisms lie behind this diversity of microscopic pathways to patterning remains open.

Unlike the self-assembly of colloidal particles, pattern formation in motile microorganisms and other living matter is typically driven by non-equilibrium rather than thermodynamic forces. Indeed, the dynamics of both dilute and concentrated bacterial fluids is already known to be vastly different from that of a suspensions of Brownian particles. For instance, suspensions of active, self-propelled particles, have been predicted to exhibit giant density fluctuations [12, 13], which have been observed experimentally [14]. Similarly, an initially uniform suspension of self-propelled particles performing a “run-and-tumble” motion like *E. coli* has recently been shown theoretically to separate into a bacteria-rich and a bacteria-poor phase, provided that the swimming speed decreases sufficiently rapidly with density [15]. This is akin to what happens in the spinodal decomposition of binary immiscible fluids, but has no counterpart in a system of Brownian particles interacting solely by density-dependent diffusivity. (The latter obey the fluctuation-dissipation theorem, ensuring that the equilibrium state

is diffusivity-independent.) Other non-equilibrium effects, such as ratchet physics, have also been observed and used either to rectify the density of bacteria [16–18] or to extract work from bacterial assemblies [19].

Some aspects of bacterial patterning show features common to other nonequilibrium systems, and a crucial task is to identify the key ingredients that control their development. In many equilibrium and nonequilibrium phase transitions an initial instability creates density inhomogeneities; these coarsen, leading eventually to macroscopic phase separation [20]. The situation observed in bacterial assemblies often differs from this; long-lived patterns emerge with fixed characteristic length scales, suggesting that any underlying phase separation is somehow arrested. The strong diversity of biological functions met in experiments has led to an equally diverse range of proposed phenomenological models [5–7, 9–11] to account for such effects. Most of them rely on the coupling of bacteria with external fields (food, chemoattractant, stimulant, etc.), and many involve a large number of parameters due to the complexity of the specific situation of interest. The most common mechanism used to explain the bacterial patterns is chemotaxis [6]: the propensity of bacteria to swim up/down gradients of chemoattractants/repellants. This explanation is so well established in the literature for at least two organisms (*E. coli* and *S. typhimurium* [6]) that observation of similar patterns in other species might defensively be taken as evidence for a chemotactic phenotype.

Here we identify a very general mechanism that can lead to pattern formation in bacterial colonies and which may encompass a large class of experimental situations. This mechanism involves a density-dependent motility, giving rise to a phase separation which is then arrested, on a well defined characteristic length scale, by the birth and death dynamics of bacteria. For definiteness we will work this through for a particular model of bacte-

rial run-and-tumble motion, involving a swim speed that depends (via unspecified interactions) on local bacterial density. This gives pattern similar to those observed in experiments [5, 6]. However, the basic mechanism—density-dependent motility coupled to logistic population growth—is not limited to this example. Our work demonstrates that chemotaxis *per se* is not a prerequisite for observing what are sometimes colloquially referred to as ‘chemotactic patterns’.

It is indeed remarkable that density-dependent swim speed and logistic growth alone are sufficient to create some of the specific pattern types previously identified with specific chemotaxis mechanisms. In mechanistic terms, we find that the logistic growth dynamics effectively arrests a spinodal phase separation that is known to follow from a density-dependent swim speed [15]. Put differently, an initially uniform bacterial population with small fluctuations will aggregate into droplets, but these will not coarsen further once a characteristic length scale is achieved, at which aggregation and birth/death effects come into balance. Starting instead from a small inoculum, we predict formation of concentric rings which, under some conditions, at least partially break up into spots at late times [5].

To exemplify our generic mechanism we will start from a minimal model of run-and-tumble bacteria, that can run in straight lines with a swim speed v and randomly change direction at a constant tumbling rate τ^{-1} [21, 22]. To this we add our two key ingredients: a local density-dependent motility, and the birth/death of bacteria, the latter accounted for through a logistic growth model. Of course, bacteria can interact locally in various ways, ranging from steric collisions [15] to chemical quorum-sensing [6]. (Indeed a nonspecific dependence of motility on bacterial density was previously argued to be central to bacterial patterning by Kawasaki [8].) Here we focus on the net effect of all such interactions on the swim speed $v(\rho)$, which we assume to decrease with density ρ . This dependence might include the local effect of a secreted chemoattractant (such as aspartate [3–5] which causes aggregation, effectively decreasing v) but does not assume one.

In addition to their run-and-tumble motion, real bacteria continuously reproduce, at a medium-dependent growth rate which ranges from about one reciprocal hour in favourable environments such as *Luria broth* to several orders of magnitude lower for ‘minimal’ media such as M9. In bacterial colonies patterns may evolve on timescales of days [6], over which such population growth dynamics can be important.

We now derive continuum equations for the local density $\rho(\mathbf{r}, t)$ in a population of run-and-tumble bacteria, with swim speed $v(\rho)$, growing at a rate $\alpha(1 - \rho/\rho_0)$. The latter represents a sum of birth and death terms, in balance only at $\rho = \rho_0$. At large scales in a uniform system, the motion of individual bacteria is characterized by a diffusivity $D(\rho) = v(\rho)^2\tau/d$, where τ^{-1} is the tumbling rate and d the dimensionality [21, 22]. Crucially how-

ever, a non-uniform swimming speed $v(\mathbf{r})$ also results in a mean drift velocity $V = -v\tau\nabla v$ [21] which here gives $V = -D'(\rho)\nabla\rho/2$ [15]. This contribution is crucial to phase separation [15] and will again play a major role here. However this term has no counterpart in ordinary Brownian motion (even if particles have variable diffusivity) and was accordingly overlooked in previous studies which relied on phenomenological equations involving a density-dependent diffusivity and no drift [8].

Coupling the diffusion-drift equation for run-and-tumble bacteria, as derived in [15], with the logistic growth term, the full dynamics is then given by:

$$\frac{\partial\rho(\mathbf{r}, t)}{\partial t} = \nabla \cdot [\mathcal{D}_e(\rho)\nabla\rho(\mathbf{r}, t)] + \alpha\rho(\mathbf{r}, t) \left(1 - \frac{\rho(\mathbf{r}, t)}{\rho_0}\right) - \kappa\nabla^4\rho(\mathbf{r}, t) \quad (1)$$

where the ‘effective diffusivity’ is

$$\mathcal{D}_e(\rho) = D(\rho) + \frac{1}{2}\rho D'(\rho) \quad (2)$$

This results from the summed effects of the true diffusive flux $-D(\rho)\nabla\rho$ and the non-linear drift flux ρV . In Eq.(1) we have also introduced a phenomenological surface tension $\kappa > 0$, which controls gradients in the bacterial density. Such a contribution has been shown to arise when the speed of a bacterium depends on the average density in a small local region around it, rather than a strictly infinitesimal one [15]. Eq. (1) neglects noise, both in the run-and-tumble dynamics and in the birth/death process. The former noise source conserves density and should become irrelevant at the experimental time scale of days. On the other hand, the non-conservative noise in the birth and death dynamics may be more important, and we have verified that our results are robust to its introduction at small to moderate levels. Numerical simulations of Eq. (1) have been performed with standard finite difference methods (although noise does require careful treatment, as in [23, 24]), with periodic boundary conditions used throughout. For definiteness, all our simulations have been carried out with $v(\rho) = v_0e^{-\lambda\rho/2}$, where $v_0 > 0$ is the swim speed of an isolated bacterium and $\lambda > 0$ controls the decay of velocity with density. The precise form of $v(\rho)$ is however not crucial for the phenomenology presented here, and the instability analysis offered below does not assume it.

The logistic population dynamics alone would cause the bacterial density to evolve toward a uniform density, $\rho(\mathbf{r}) = \rho_0$, which constitutes a fixed point for the proposed model. Although this homogeneous configuration is stable in the absence of bacterial interactions, it has been shown [15] that, without logistic growth, a density-dependent swim speed $v(\rho)$ leads to phase separation via a spinodal instability whenever $dv/d\rho < -v/\rho$. By Eq. (2) this equates to the condition $\mathcal{D}_e < 0$, and it is indeed obvious that the diffusive part of Eq. (1) is unstable for negative \mathcal{D}_e . It is important, clearly, that

\mathcal{D}_e can be negative although D is not. This holds for a much wider class of nonequilibrium models than the one studied here; we return to this point at the end of the paper.

For the choice of $v(\rho)$ made in our simulations, we have $\mathcal{D}_e = D(\rho)[1 - \rho\lambda/2]$ and the flat profile will thus become unstable for ρ_0 above $2/\lambda$. We have confirmed this numerically, and find that upon increasing ρ_0 , the uniform state becomes (linearly) unstable, evolving in a 1D geometry into a series of “bands” of high bacterial density separated by low density regions. Depending on the parameters, this transition can be continuous (supercritical), with the onset of a harmonic profile whose amplitude grows smoothly with ρ_0 , or discontinuous (subcritical) with strongly anharmonic profiles (see Fig. 1).

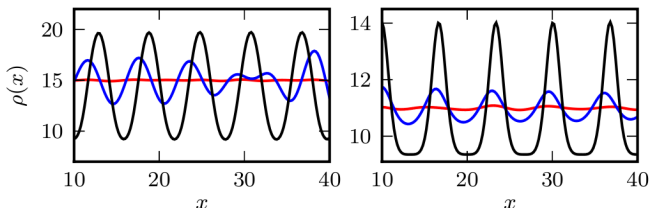


Figure 1: Growth of the instability in the supercritical (left) and subcritical cases (right). The three lines correspond to three successive times. A small perturbation around ρ_0 (red line) growth toward harmonic or anharmonic patterns in the supercritical or subcritical case, respectively. **Left:** Supercritical case ($\alpha = \kappa = 0.01$, $\lambda = 0.02$, $\rho_0 = 15$, $D_0 = 1$, times: 10^2 , 10^3 , 10^4). **Right:** Subcritical case ($\alpha = \kappa = 0.005$, $\lambda = 0.02$, $\rho_0 = 11$, $D_0 = 1$, times: $3 \cdot 10^2$, $3 \cdot 10^3$, 10^5)

The transition to pattern formation arising from Eq. (1) is a fully nonequilibrium one: it is not possible to write down an effective thermodynamic free energy which would lead to this equation of motion. Nonetheless, it is possible to understand why the birth/death process effectively arrests the spinodal decomposition induced by the density-dependent swim speed. The latter tends to separate the system into high and low density domains with densities either side of ρ_0 . (Without the logistic term, these would coarsen with time.) Bacteria thus tend to be born in the low density regions and to die in the high density regions. To maintain a steady state, they have to travel from one to the other: balancing the birth/death terms by the diffusion-drift transport flux between the domains then sets a typical scale beyond which domain coarsening can no longer progress. Were any domain to become much larger, the density at its centre would soon regress towards ρ_0 , re-triggering the spinodal instability locally. (This is closely reminiscent of what happens in a thermodynamic phase separation when the supersaturation is continuously ramped [25].)

To better understand the onset of the instability, let us linearize Eq. (1) around $\rho(\mathbf{r}) = \rho_0$ and work in Fourier space. Defining $\rho(\mathbf{r}) = \rho_0 + \sum_q \delta\rho_q \exp(i\mathbf{q} \cdot \mathbf{r})$ yields:

$$\dot{\delta\rho}_q = \Lambda_q \delta\rho_q; \quad \Lambda_q = -\alpha - q^2 \mathcal{D}_e(\rho_0) - \kappa q^4 \quad (3)$$

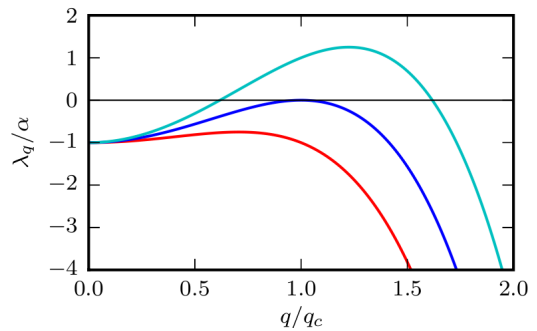


Figure 2: Three plots of $\Lambda_q(q)$ for $|\mathcal{D}_e(\rho_0)|/\sqrt{\alpha\kappa} = 1; 2; 3$. At the transition, only one critical mode $q = q_c$ is unstable.

The flat profile $\rho = \rho_0$ is thus stable if $\Lambda_q \leq 0$ for all q and is unstable otherwise. From the expression for $\mathcal{D}_e(\rho_0)$, Eq. (2), one sees that instability occurs if

$$\Phi \equiv -\frac{\rho_0 D'(\rho_0)}{2D(\rho_0)} \geq 1 \quad \text{and} \quad -\frac{\mathcal{D}_e(\rho_0)}{\sqrt{\alpha\kappa}} \geq 2 \quad (4)$$

At the onset of the instability only one mode is unstable, with wavevector $q_c = \sqrt{2\alpha/|\mathcal{D}_e(\rho_0)|}$, as can be seen in Figure 2. The first condition in Eq. (4), $\Phi \geq 1$, is equivalent to the requirement that $\mathcal{D}_e < 0$ given previously. From the dispersion relation, Eq. (3), we see that the resulting destabilization is balanced by the stabilizing actions of bacterial reproduction and the surface tension at large and small wavelength, respectively. The unstable modes thus lie within a band $q_1 < q < q_2$ where $q_1 \simeq q_\alpha \equiv \sqrt{\alpha/|\mathcal{D}_e(\rho_0)|}$ and $q_2 \simeq q_\kappa \equiv \sqrt{|\mathcal{D}_e(\rho_0)|/\kappa}$ set the wavelengths below and above which the stabilizing effects of bacteria reproduction and the surface tension can compete with the destabilizing effect of the negative diffusivity, respectively. For unstable modes to exist, one needs $q_1 \leq q_2$; restoring prefactors, this yields $2q_\alpha \leq q_\kappa$ which is the second criterion in Eq. (4). This analysis is consistent with the view that phase separation is arrested by the birth/death dynamics, which stabilizes the long wavelength modes ($\Lambda_0 = -\alpha$), while the phenomenological tension parameter κ primarily fixes the interfacial structure of the domains, not their separation.

We now consider more closely the parameters controlling the transition to pattern formation. For definiteness, we address the specific case used for our simulations, $D(\rho) = D(0) \exp(-\lambda\rho)$. To put Eq. (1) in dimensionless form, we define rescaled time, space and density as

$$\tilde{t} = \alpha t; \quad \tilde{\mathbf{r}} = \left(\frac{\alpha}{\kappa}\right)^{1/4} \mathbf{r}; \quad u = \frac{\rho}{\rho_0} \quad (5)$$

The equation of motion now reads

$$\dot{u} = \nabla \cdot [R e^{-2\Phi u} (1 - \Phi u) \nabla u] + u(1 - u) - \nabla^4 u \quad (6)$$

where $R \equiv D_0/\sqrt{\alpha\kappa}$ and $\Phi = \lambda\rho_0/2$ are the two remaining dimensionless control parameters. Meanwhile the conditions (4) for pattern formation become

$$\Phi \geq 1; \quad R \geq R_c = 2 \frac{\exp(2\Phi)}{\Phi - 1} \quad (7)$$

These relations, combined with the preceding linear stability analysis, define a phase diagram in the (R, Φ) plane (Figure 3) that agrees remarkably well with numerical results for systems prepared in a (slightly noisy) uniform initial state.

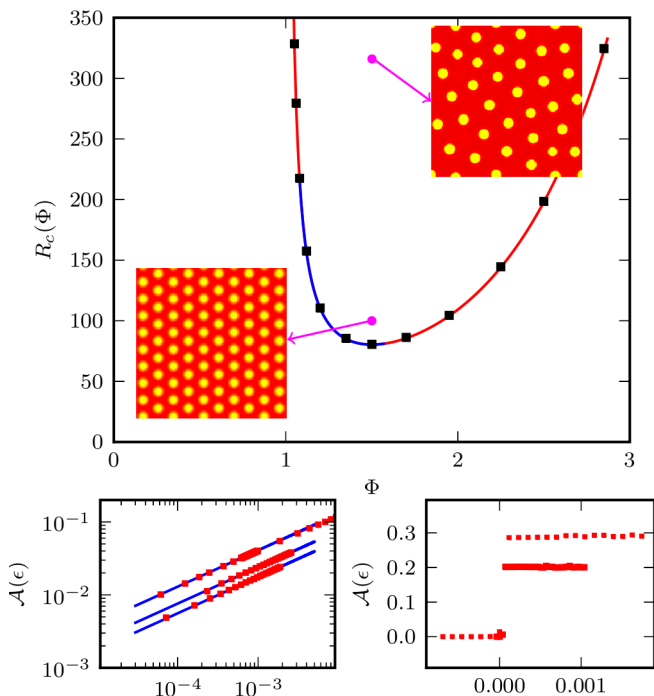


Figure 3: **Top:** Phase diagram in the (R, Φ) plane. The outer region corresponds to stable behavior whereas within the curve, patterning occurs. The solid line is the theoretical phase boundary – Eq (7) – which accurately fits the numerics (black squares). The blue and red sections correspond to continuous and discontinuous transitions respectively. The two magenta dots correspond to two 2D simulations which show ordered harmonic patterns close to supercriticality and amorphous patterns otherwise. **Bottom-left:** Transition in the supercritical regime. The blues lines correspond to the theory – Eq (8) – whereas the squares comes from simulations ($\Phi = 1.5; 1.35; 1.2$ from top to bottom). **Bottom-right:** Transition in the subcritical regime for $\Phi = 1.06$ and $\Phi = 1.7$ (bottom to top).

Close to the transition, the emergent steady-state pattern can be studied using an amplitude equation (see Supporting Information). Introducing $\varepsilon = (R - R_c)/R_c$, one gets in 1D that for $1.08 \leq \Phi \leq 1.58$, the transition is supercritical (continuous) and the steady state is given by

$$u \simeq 1 + \mathcal{A}(\varepsilon) \cos(x);$$

$$\mathcal{A}^2(\varepsilon) = \varepsilon \frac{18(1 - \Phi)^2}{34\Phi^4 - 56\Phi^3 - 24\Phi^2 + 31\Phi + 19} \quad (8)$$

which agrees with simulations (Fig 3, bottom left). Outside this range, the transition becomes subcritical (discontinuous, Fig 3, bottom right) and the analytical tools

available become less reliable [26]. We emphasize again that the basic mechanism for patterning presented above does not depend on the precise form chosen for $v(\rho)$. Quantitatively however, Eq. (8), and the frontier between subcriticality and supercriticality, do depend on the details of the interplay between the nonlinearity in $v(\rho)$ and the logistic growth term. We leave further analysis of such model-specific features to future work.

While the amplitude equation is more easily developed in 1D, the stability analysis offered above is valid in higher dimensions and it is natural to ask what happens in 2D, which is the relevant geometry for Petri dish studies with growing bacterial colonies. Fig. 4 shows the simulated time evolution of $\rho(\mathbf{r}, t)$ for a system started with small random fluctuations around the equilibrium density ρ_0 , with other parameters as in Fig. 1. Perhaps not surprisingly, bands are replaced by droplets of the high density phase dispersed in a low density background at large times. This is the typical steady state obtained with a near-uniform starting condition. However, the structure and organization of the bacterial drops in the steady state depends on the point (R, Φ) chosen in the phase diagram. Generally, the closer the system is to the supercritical instability curve, the more ordered the patterns. For instance we have observed an essentially crystalline distribution of bacterial drops, which develops defects and eventually becomes amorphous on moving further away from the phase boundary (Fig. 3, insets to main panel). For particular choices of parameters, our model can also admit other steady state patterns. Close to the supercritical line, where the phase transition is continuous, we can obtain long-lived stripes, whereas for fixed large values of R and Φ close to the (right) subcritical phase boundary, we have also observed ‘inverted droplets’ with a high density lawn punctuated by low density ‘holes’.

In these 2D geometries initialized from a near-uniform state, droplets can coalesce in the early stages, while at late times the dynamics is governed by evaporation-condensation events (see Figs. 4 and 5). However it is already apparent from Fig. 4 that coarsening eventually stops and the droplets reach rather well-defined steady state sizes and centre-to-centre distances. This can be quantified by looking at the time evolution of the characteristic domain size, $L(t)$, which we have computed as the inverse of first moment (times 2π) of the structure factor [20]. Fig. 5 suggests that $L(t)$ at late times eventually stops increasing and reaches a steady state value. (The visible steps in domain size mark discrete evaporation events involving smaller bacterial droplets; presumably $L(t)$ would become smooth for a large enough system.)

These droplet patterns in steady state are very similar to those observed for *E. coli* in a liquid medium or *S. typhimurium* in semi-solid agar (0.24% water-agar in Ref. [5]) when starting from a uniform distribution [6]. For the *E. coli* case, interactions are believed to come from chemoattractant, emitted by the bacteria them-

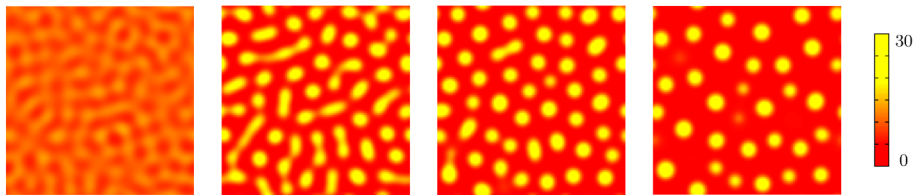


Figure 4: Numerical results for a 2D simulation with size equal to 16×16 , $\lambda = 0.3$, $D_0 = 1$, $\alpha = 0.01$, $\kappa = 0.001$ and $\rho_0 = 10$. Times corresponding to the snapshots are (in simulation units, from left to right): 5, 12, 19.6 and 50.6.

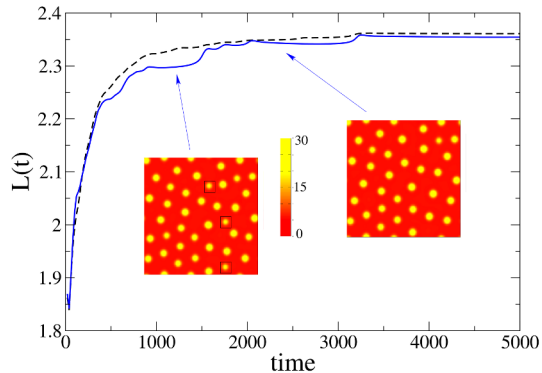


Figure 5: Plot of the characteristic domain size, $L(t)$ as a function of time for a system in the inhomogeneous phase, with initially random density fluctuations around ρ_0 . Parameters were: $\alpha = 0.01$, $\lambda = 0.27$, $\kappa = 0.001$, while the system size was 20×20 . The solid line corresponds to a single run, while the dashed line is an average over 6 runs. The steps in the single run curve correspond to evaporation-condensation events, highlighted by black squares in the snapshots shown in the figure (before and after one of the steps respectively, arrows indicate positions on the plot corresponding to the two snapshots).

selves, that is not degraded over time [3, 4]. The chemoattractant distribution should become more and more uniform so that these interactions decay to zero as time proceeds. In our framework this is analogous to decreasing Φ , which will turn any initially unstable state into a homogeneous one, and can thus explain that the patterns observed experimentally fade with time (whereas in our simulations Φ remains constant and the pattern are stable indefinitely). *E. coli* in a semi-solid medium also exhibits droplet patterns of high symmetry. In our framework, such patterns result from a continuous transition, close to the supercritical line.

The growth of bacterial colonies of *S. typhimurium* starting from a small inoculum of bacterial cells in semi-solid agar leads to quite specific (transient but long-lived) patterns, with the bacteria accumulating in concentric rings that can subsequently fragment into a pattern of dots [5, 6]. Once again, although these patterns are believed to stem from a chemotactic mechanism [6], we find they can arise in principle without one, so long as our two basic ingredients of density-suppressed motility and logistic growth are both present. Indeed, initializing

our simulations with a single small droplet of high density ρ , we find that a similarly patterned bacterial colony structure develops. First, the bacteria spread radially (through a Fisher-like wave), forming an unstructured lawn with the highest density at the center. This background density increases logistically until the onset of instability via our generic phase-separation mechanism; with circular symmetry, the instability causes concentric rings of high bacterial density to successively develop that are very stable in time (Figs. 6c and 6d). The patterns observed at later times again depend on the position of the parameters in the (R, Φ) plane. If we fix a value of R , e.g. 100, larger values of Φ in the unstable region lead to rings being very stable. For smaller values of Φ , on the other hand, effectively corresponding to weaker interactions between the bacteria, we observe that rings initially form but rapidly destabilize through a secondary modulation of the bacterial density along them. This eventually breaks the rings into a series of drops. The inner rings destabilize first, and the system evolves eventually to the same steady state as found starting from a uniform density, composed of drops with well defined characteristic size and separation. All this phenomenology is strikingly reminiscent of the dynamics observed by Woodward *et al* [5] for *S. typhimurium*, where rings are stable at large concentrations of potassium succinate (a ‘stimulant’ which promotes pattern formation), but break up into drops at smaller ones. Our model shows a similar morphological change when decreasing Φ , i.e. the strength of the interactions.

Different views are possible concerning the ability of our generic model to reproduce the observed chemotactic patterns of *E. coli* and *S. typhimurium* [6]. One possibility is that Eq. (1), with the interpretation we have given for it, actually does embody the important physics of pattern formation in these organisms. Indeed it is well accepted that bacteria in the high density concentric rings are essentially non-motile [27]. The precise mechanism leading to this observation is not well understood [6], but it is possible that the chemotactic mechanism mainly acts to switch off motility at high density. If so, by focussing solely on this aspect (with a correspondingly vast reduction in the parameter space from that of explicit chemotactic models [5, 6]) our model might capture the physics of these chemotactic patterns in a highly economical way. Interestingly, our model is essentially local, whereas chemotaxis in principle mediates

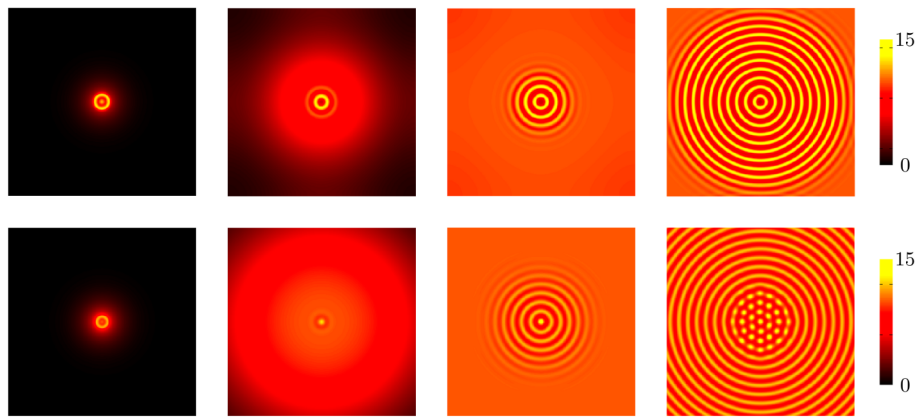


Figure 6: Dynamics of formation of "chemotactic patterns" in 2D, starting from a single small bacterial droplet in the middle of the simulation sample. Top row: Formation of "chemotactic rings" in a system with $\alpha = 0.1$, $\lambda = 0.33$, and $\kappa = 0.001$. The simulation box has size 40×40 . The snapshots correspond to times equal to (in simulation units, from left to right) 10, 50, 100 and 270. Bottom row: Breakage of "rings" into "dots". The four snapshots correspond to the time evolution of a system with $\alpha = 0.1$, $\lambda = 0.26$, and $\kappa = 0.001$. We show a 40×40 fraction of the simulation box, with the boundaries far away and not affecting the pattern. The snapshots correspond to times equal to (in simulation units, from left to right) 10, 70, 290 and 1220.

interactions between bacteria that are nonlocal in both space and time. It is not clear whether such nonlocality is essential for the chemotactic models in [5, 6] or if fast-variables approximations and gradient expansions would reduce these models (which involve between 9 and 12 parameters) into Eq.[1]. In this case, we would still have in Eq.[1] a highly economical model for chemotactic pattern-formation organisms, possibly with a different interpretation of \mathcal{D}_e and κ .

Alternatively, the success of our local model for these chemotactic organisms might be largely coincidental. But in that case, such a sparse model should be easily falsified, for instance by using the linear stability analysis to relate the typical length scale of the patterns to microbial parameters. This length scale is of order $2\pi/q_c = 2\pi\sqrt{|\mathcal{D}_e|/\alpha}$, with $|\mathcal{D}_e| \simeq D$, a typical bacterial diffusion coefficient ($D \sim \mathcal{O}(100 \mu\text{m}^2\text{s}^{-1})$ for *E. coli* [22]). Using the previously quoted growth rate $\alpha \simeq 1 \text{ hr}^{-1}$, we get a ring separation of $\sim 1 \text{ mm}$, in order-of-magnitude agreement with the experimental value [5]. This test could perhaps be sharpened usefully by altering the growing medium so as to change α .

More generally, our analysis of Eq. (1) shows that the main prerequisite for pattern formation, assuming the presence the logistic growth term, is negativity of the effective diffusion constant \mathcal{D}_e . For run-and-tumble dynamics, $\mathcal{D}_e < 0$ was shown to arise for a sufficiently strong decay of swim-speed with density; it does so because spatial variations in the true diffusivity $D(\rho)$ create a drift flux $\rho V = -\rho D'(\rho)\nabla\rho/2$ which can overcompensate the true diffusive flux $-D\nabla\rho$ [15]. Negative \mathcal{D}_e could, however, equally arise for any density dependent nonequilibrium diffusion process. Indeed, the principle of detailed balance, which holds only for equilibrium systems, leads to the Einstein relation, that $D = k_B T \mu$

with D a many-body diffusivity and μ the corresponding mobility. This alone ensures that no drift velocity can arise purely from gradients in D . In nonequilibrium systems, one should expect generically to find such drift velocities, and the run-and-tumble model is merely one instance of this. Accordingly one can expect in principle to find cases of negative \mathcal{D}_e in other microorganisms showing distinctly different forms of density-dependent self-propulsion.

To summarize, we have studied the dynamics of a system of reproducing and interacting run-and-tumble bacteria, in the case where interactions lead to a decreasing local swim speed with increasing local density. We have thereby identified a potentially generic mechanism for pattern formation in which an instability towards phase separation, caused by the tendency for bacteria to move slowly where they are numerous, is arrested by the birth and death dynamics of bacterial populations. We have shown that these two ingredients alone are enough to capture many of the patterns observed experimentally in bacterial colonies – including some that have only previously been explained using far more complex models involving specific chemotactic mechanisms. Indeed, if motility decreases steeply enough with density, then a spatially homogeneous bacterial population becomes unstable to density fluctuations leading to the formation of bands (1D) or droplets (2D). The length scale of the resulting pattern is set by a balance between diffusion-drift fluxes and the logistic relaxation of the population density towards its fixed-point value. Starting instead from a small initial droplet of bacteria, we predict the formation of concentric rings, each of which may eventually further separate into droplets.

In several well studied systems, such characteristic patterns are (with good reason) believed to be the direct

result of chemotactic behavior [5, 6]. It is therefore remarkable that they can also arise purely from the interplay of density-dependent diffusivity and logistic growth, without explicit reference to the dynamics (or even the presence) of a chemoattractant. This suggests that similar patterns might arise in organisms having no true chemotactic behavior at all. Such patterns could then be the result of local chemical signalling without gradient detection (quorum-sensing, not chemotaxis) or even purely physical interactions (steric hindrance), either of which could in principle produce the required dependence of motility on density. Last, a motility decreasing with density is only one of the many mechanism that could lead to $\mathcal{D}'_e(\rho) < 0$ and our analysis would apply equally to all such cases.

The simplest version of our model allows identification of just two dimensionless parameters that control the entire pattern-forming process. In both homogeneous and centrosymmetric geometries, this gives predictions for how the pattern type depends on interaction strength which are broadly confirmed by experimental data. This suggests that some of the diverse patterns formed by colonies of motile bacteria could have a relatively universal origin.

Acknowledgments

We thank Otti Croze for discussions. We acknowledge funding from EPSRC EP/E030173. MEC holds a Royal Society Research Professorship. IP acknowledges the Spanish MICINN for financial support (FIS2008-04386).

Appendix A

We show here how to derive the amplitude equation (8). Let us start from the dimensionless equation of motion (6)

$$\dot{u} = \nabla[Re^{-2\Phi u}(1 - \Phi u)\nabla u] + u(1 - u) - \nabla^4 u \quad (\text{A1})$$

and recall the two conditions for patterning Eq. (7):

$$\Phi > 1; \quad R \exp(-2\Phi)(\Phi - 1) > 2 \quad (\text{A2})$$

To analyze precisely the transition, we derive below the steady-state limit of the amplitude equation in 1D. By inspection one sees that the unperturbed steady-state of (A1) is given by $u = 1$. To characterize the amplitude of the perturbation around $u = 1$, we introduce $u = 1 + w/\Phi$ so that w evolves with

$$\dot{w} = -\partial_x[Re^{-2\Phi}(\Phi-1)(1+\frac{w}{\Phi-1})e^{-2w}\partial_x w] - w(1+\frac{w}{\Phi}) - \partial_x^4 w \quad (\text{A3})$$

We are interested by the vicinity of the transition where

$$Re^{-2\Phi}(\Phi - 1) = 2(1 + \varepsilon) \quad (\text{A4})$$

for $\varepsilon > 0$ and small. The dynamics now reads

$$\dot{w} = \mathcal{L}w - 2\varepsilon\partial_x^2 w + g(w) \quad (\text{A5})$$

where $\mathcal{L} = -(1 + \partial_x^2)^2$ is the linear part of the evolution operator *at the transition*, $2\varepsilon\partial_x^2 w$ gives an extra linear part due to the perturbation ($\varepsilon > 0$) and $g(w)$ is the non-linear part:

$$g(w) = -\frac{w^2}{\Phi} - \partial_x \left[2(1 + \varepsilon) \left(\left(1 + \frac{w}{\Phi - 1} \right) e^{-2w} - 1 \right) \partial_x w \right] \quad (\text{A6})$$

1. Amplitude equation

As usual with the amplitude equation approach, we expand w in power series of the perturbation ε and study Eq. (A5) order by order. As shown below (Eqs (21-23)), the correct expansion is

$$w = U_0\varepsilon^{1/2} + U_1\varepsilon + U_2\varepsilon^{3/2} + \dots \quad (\text{A7})$$

Expanding (A6) to the order $\varepsilon^{3/2}$ and substituting in (A5) yields order by order:

$$-\mathcal{L}U_0 = 0 \quad (\text{A8})$$

$$-\mathcal{L}U_1 = -\frac{U_0^2}{\Phi} - \frac{3 - 2\Phi}{\Phi - 1} \partial_x^2 U_0^2 \quad (\text{A9})$$

$$-\mathcal{L}U_2 = -2\partial_x^2 U_0 - \frac{2U_0U_1}{\Phi} - \frac{3 - 2\Phi}{\Phi - 1} 2\partial_x^2 U_0U_1 - \frac{4}{3} \frac{\Phi - 2}{\Phi - 1} \partial_x^2 U_0^3 \quad (\text{A10})$$

Equation (A8) can be easily solved and yields

$$U_0 = Ae^{ix} + A^*e^{-ix} \quad (\text{A11})$$

The amplitude of the perturbation we are trying to derive is thus $2|A|$. Equation (A9) can also be solved directly:

$$U_1 = Be^{ix} + B^*e^{-ix} + C + De^{2ix} + D^*e^{-2ix} \quad (\text{A12})$$

where B can be determined from higher order equations (but does not interest us here), and C and D are given by

$$C = -\frac{2|A|^2}{\Phi}; \quad D = \frac{A^2}{9} \left(4\frac{3 - 2\Phi}{\Phi - 1} - \frac{1}{\Phi} \right) \quad (\text{A13})$$

as can be checked by direct substitution in Eq. (A9). Equation (A10) does not always have a solution. Indeed, the application of \mathcal{L} to any function U_2 cannot yield a multiple of e^{ix} , (since $\mathcal{L}e^{ix} = 0$ and \mathcal{L} is linear). The r.h.s. however does contain a multiple of e^{ix} whose prefactor must thus vanish. This gives a condition for the expansion to provide a proper steady-state solution of the problem. Let us summarize the contributions of

the different terms to the prefactor of e^{ix} in the r.h.s of Eq. (A10)

$$-2\partial_x^2 U_0 \text{ yields } 2A \quad (\text{A14})$$

$$\left(\frac{3-2\Phi}{\Phi-1}2\partial_x - \frac{2}{\Phi}\right)U_0U_1 \text{ yields } 2A|A|^2\left(\frac{3-2\Phi}{\Phi-1} - \frac{1}{\Phi}\right) \quad (\text{A15})$$

$$\begin{aligned} &\times \left(\frac{1}{9}\left(4\frac{3-2\Phi}{\Phi-1} - \frac{1}{\Phi}\right) - \frac{2}{\Phi}\right) \\ -\frac{4}{3}\frac{\Phi-2}{\Phi-1}\partial_x^2 U_0^3 \text{ yields } 4\frac{\Phi-2}{\Phi-1}A|A|^2 \end{aligned} \quad (\text{A16})$$

The sum of these terms vanishes only if

$$A\left(9\Phi^2(\Phi-1)^2 + 2|A|^2(34\Phi^4 - 56\Phi^3 - 24\Phi^2 + 31\Phi + 19)\right) = 0 \quad (\text{A17})$$

and thus either

$$A = 0; \quad \text{or} \quad |A|^2 = \frac{9\Phi^2(1-\Phi)^2}{2(34\Phi^4 - 56\Phi^3 - 24\Phi^2 + 31\Phi + 19)} \quad (\text{A18})$$

Finally, the first order in the amplitude equation yields

$$w(x) = 2|A|\sqrt{\varepsilon}\cos(x-x_0) \quad (\text{A19})$$

where x_0 is a constant. Note that by construction $|A|^2 > 0$ and a non-zero solution only exists for $\Phi \in [1.08439, 1.59237]$. For these values of Φ , Eq. (A18) and (A19) work very well, as can be checked in figure 7. Outside this range the transition becomes subcritical and the standard approach does not work anymore. Alternative treatments have been proposed but are not as reliable (see ref [20] for more details). Interestingly, we see that the order of the transition and the amplitude of the perturbation depend on how non-linear terms in $g(w)$ balance the linear growth term $-2\varepsilon\partial_x^2 w$ in (A5). Since the former depends on the non-linear relation $v(\rho)$, we do not expect equation (A18) to be generic, as opposed to the stability analysis which can be expressed solely in terms of $\mathcal{D}_e(\rho_0)$ and its derivative.

2. What is the correct expansion?

In (A7), we expanded w in power series of $\sqrt{\varepsilon}$, thus assuming that the amplitude is an analytic function of

$\sqrt{\varepsilon}$. One could look for a more general expansion:

$$w = U_0\varepsilon^\alpha + U_1\varepsilon^{2\alpha} + U_2\varepsilon^{3\alpha} \quad (\text{A20})$$

In this case, the expansion of equation (A5) yields two power series: $\sum R_k\varepsilon^{\alpha k}$ and $\sum W_k\varepsilon^{\alpha k+1}$. For the two series to give terms that can balance each-other, one needs $\alpha + 1 = k\alpha$ for $k \geq 2$ and thus

$$\alpha = \frac{1}{k-1} \quad (\text{A21})$$

The candidates for α are thus 1; 1/2; 1/3; ... Note that $\alpha \leq 1$ implies $2\alpha + 1 \geq 3\alpha$. We can therefore stop the expansion at 3α and $2\alpha + 1$ to get the first three terms in the expansion of equation (A5)

Let us first try $\alpha = 1$. The order by order the expansion yields

$$L^2 U_0 = 0, \quad \mathcal{O}(\varepsilon) \quad (\text{A22})$$

$$L^2 U_1 = -\frac{U_0^2}{\Phi} - \frac{3-2\Phi}{\Phi-1}\partial_x^2 U_0^2 - 2\partial_x^2 U_0, \quad \mathcal{O}(2\varepsilon) \quad (\text{A23})$$

Equation (A22) yields $U_0 = Ae^{ikx} + A^*e^{-ikx}$ but equation (A23) cannot be solved since there is a non-zero multiple of e^{ikx} on the r.h.s. ($-2\partial_x^2 U_0$) which cannot result from the application of L^2 to any function. Thus $\alpha = 1$ is not an option.

For $\alpha \leq 1/3$, then $\alpha + 1 > 1 \geq 3\alpha$. There is thus no contribution of $-2\varepsilon\partial_x^2 w$ to the first three orders in the expansion of (A5). In particular, the two first order are still given by (A8) and (A9), whereas the third order is given by (A10) without the term linear in U_0 . This means that the contribution (A14) is not present and the prefactor of e^{ikx} in the r.h.s. of (A10) only contains multiples of $|A|^2 A$. The resolvability condition (A17) is thus of the form $A|A|^2 f(\Phi) = 0$ which implies $|A| = 0$. The only expansion which yields a result is thus for $\alpha = 1/2$.

[1] Shapiro J. A. (1995) The significance of bacterial colony patterns. *BioEssays* 17: 597-607.
[2] Harshey R. M. (2003) Bacterial motility on a surface: Many ways to a common goal. *Ann. Rev. Microbiol.* 57:249-273.
[3] Budrene E. O., Berg H. C. (1991) Complex patterns formed by motile cells of *Escherichia-coli*. *Nature* 349: 630-633.
[4] Budrene E. O., Berg H. C. (1995) Dynamics of formation of symmetrical patterns by chemotactic bacteria. *Nature*

376:49-53.

[5] Woodward D.E. *et al.* (1995) Spatiotemporal patterns generated by *Salmonella Typhimurium*. *Biophys. J.* 68:2181-2189.
[6] Murray J.D., *Mathematical Biology*, Vol. 2, Springer-Verlag, New York (2003).
[7] Ben-Jacob E., Cohen, I., Levine H. (2000) Cooperative self-organization of microorganisms *Adv. in Phys.* 49, 395-554.
[8] Kawasaki K. *et al* (1997) Modeling Spatio-Temporal

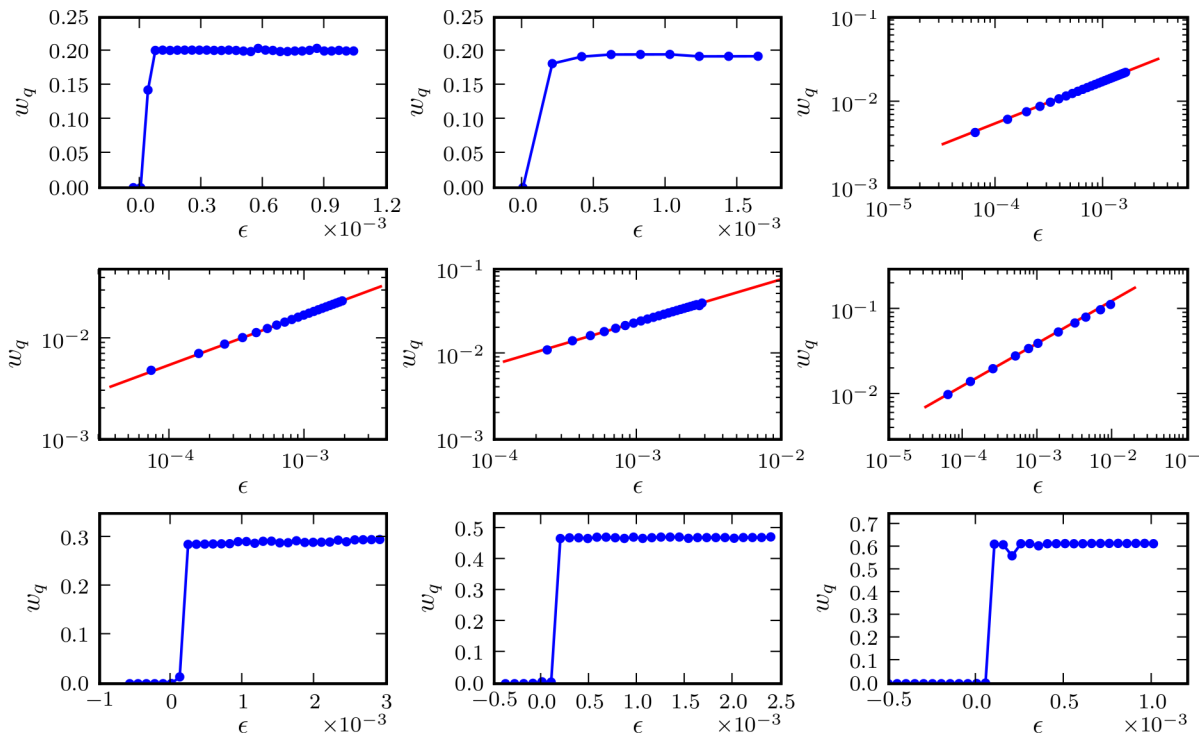


Figure 7: We simulated equation (A1) for systems of size $L = 400$ with periodic boundary conditions, using several values of Φ (From left to right, top to bottom, $\Phi = 1.06; 1.07; 1.12; 1.2; 1.35; 1.5; 1.7; 1.95; 2.5$). The steady-state $w(x)$ was then decomposed in Fourier series $w(x) = a_0 + \sum_n^{N/2} a_n \cos(2\pi nx/L) + b_n \sin(2\pi nx/L)$, where N is the number of data points and the cut-off when $n \rightarrow \infty$ is given by the Nyquist frequency. The blue points correspond to the amplitude of the largest mode: $w_q = \max_n \sqrt{a_n^2 + b_n^2}$. When the transition is continuous, we compare these points with the results of the amplitude equation $w_q = 2\sqrt{\varepsilon}|A|$, where $|A|$ is solution of (A18) (red lines) and the agreement is excellent. For $\Phi > 1.58$ or $\Phi < 1.08$, the transition is clearly discontinuous.

Patterns Generated by *Bacillus subtilis*. *J. theor. Biol.* 188:177-185.

- [9] Tyson R., Lubkin, S.R., Murray, J.D. (1999) A minimal mechanism for bacterial pattern formation. *Proc. Roy. Soc. Lon. B* 266:299-304.
- [10] Brenner, M.P., Levitov, L.S., Budrene, E.O. (1998) Physical mechanisms for chemotactic pattern formation by bacteria. *Biophys. J.* 74:1677-1693.
- [11] Espiov S.E., Shapiro J.A. (1998) Kinetic model of *Proteus mirabilis* swarm colony. *J. Math. Biol.* 36:249-268.
- [12] Toner J., Tu Y.H., Ramaswamy S. (2005) Hydrodynamics and phases of flocks. *Ann. Phys. (N.Y.)* 318: 170-244.
- [13] Ramaswamy S, Simha R.A., Toner J. (2003) Active nematics on a substrate: giant number fluctuations and long-time tails. *Europhys. Lett.* 62: 196-202.
- [14] Narayan V., Ramaswamy S., Menon N. (2007) Long-lived giant number fluctuations in a swarming granular nematic. *Science* 317: 105-108.
- [15] Tailleur J, Cates M.E. (2008) Statistical mechanics of interacting run-and-tumble bacteria. *Phys. Rev. Lett.* 100: 218103.
- [16] P. Galajda, J. Keymer, P. Chaikin, R. Austin (2008) *J. Bacteriol.* 189:8704-8707.
- [17] P. Galajda et al. (2008) Funnel ratchets in biology at low Reynolds number: choanotaxis. *J. Modern Optics* 55:3413-3422. (2008)
- [18] Tailleur J, Cates M-E (2009) Sedimentation, trapping, and rectification of dilute bacteria. *Europhys. Lett.* 86:60002.
- [19] Angelani L, Di Leonardo R, Ruocco G (2009) Self-Starting Micromotors in a Bacterial Bath. *Phys. Rev. Lett.* 102:048104.
- [20] Chaikin P.M., Lubenski T.C, *Principles of condensed matter physics*, Cambridge University Press, Cambridge (1995).
- [21] Schnitzer M.J. (1993) Theory of continuum random walks and application to chemotaxis. *Phys. Rev. E* 48:2553-2568.
- [22] Berg H.C., *E. coli in Motion*, Springer (2003).
- [23] Dickman R. (1994) Numerical study of a field theory for directed percolation. *Phys. Rev. E* 50:4404-4409.
- [24] Dornic I., Chate H., Munoz M.A. (2005) Integration of Langevin equations with multiplicative noise and the viability of field theories for absorbing phase transitions. *Phys. Rev. Lett.* 94: 100601.
- [25] Cates M.E., Vollmer J., Wagner A., Vollmer D. (2002) Phase separation in binary fluid mixtures with continuously ramped temperature. *Phil. Trans. Roy. Soc. A* 361:793-804.
- [26] P. Becherer, A.N. Morozov, W. van Saarloos, (2009) Probing a subcritical instability with an amplitude expansion: An exploration of how far one can get. *Physica D* 238:1827-1840.
- [27] Mittal N., Budrene E.O., Brenner M.P., van Oudenaar-

den, A. (2003) Motility of *Escherichia coli* in clusters formed by chemotactic aggregation. *Proc. Natl. Acad.*

Sci. USA 100:13259-13263.